ChemComm

COMMUNICATION

View Article Online
View Journal

Cite this: DOI: 10.1039/d5cc06049d

Received 24th October 2025,
Accepted 1st December 2025

DOI: 10.1039/d5cc06049d

rsc.li/chemcomm

Enzyme cascade reactions encapsulated in a liposome compartment with size-limited molecular transport

Shiwei Zhang,[a] Peng Lin,[a] Futa Komatsubara,[a] Eiji Nakata[a] and Takashi Morii *[ab]

We designed a liposome-coated DNA origami compartment to encapsulate a defined number of cascade enzymes with retained cofactors. Confinement enhanced cascade reaction efficiency particularly at low cofactor levels. Efficiency gains plateaued at higher NADH concentrations, indicating that intermediate diffusion and enzyme spatial organization influence cascade performance in confined environments.

Cellular metabolic pathways face many challenges in organizing individual enzymatic reactions, including slow turnover, loss of volatile intermediates, formation of toxic by-products, and competition for metabolites.[1] Cells overcome these limitations by compartmentalizing biomacromolecules, including enzymes, within organelles such as the nucleus, endoplasmic reticulum, and Golgi complex. These compartments create distinct microenvironments with specific pH values, ionic strengths, and polarities, thereby facilitating cascade reactions.[2] Organelle membranes act as selective barriers, while confined spaces such as carboxysomes and lysosomes[3] are thought to enhance enzyme activity by increasing the local concentration of substrates and intermediates, thereby promoting collision frequency in diffusion-driven processes.[4] In addition, the specific microenvironment and the spatial organization of multienzyme complexes enable substrate channelling, allowing direct metabolite transfer between enzymes, minimizing diffusion into the cytoplasm, reducing cross-talk with other pathways, and ultimately enhancing both efficiency and selectivity.

Synthetic compartments offer powerful platforms for mimicking such enzymatic organization by encapsulating defined metabolic pathways.[5] However, quantitatively evaluating compartmentalized enzyme cascade reactions requires compartments of controlled size and composition, as well as the precise number and arrangement of enzymes. Previous studies have examined proximity effects on substrate transfer[7] using enzymes immobilized on the DNA scaffold.[6] Nevertheless, it remains challenging to directly verifying how compartmentalization and spatial organization contribute to the efficiency of synthetic metabolic pathways, largely due to the difficulty of assembling a defined number of cascade enzymes within compartments of uniform size.

To address this challenge, we previously developed a transporting liposomal compartment with an internal DNA origami wireframe skeleton (WS), equipped with the bacterial membrane transporter, OmpF, which selectively permits passage of molecules smaller than 600 Da.[8] In the present study, we employed this platform to construct a two-step xylose cascade composed of *Talaromyces emersonii* xylose reductase (TeXR),[9] which reduces xylose to xylitol using NADH, and xylitol dehydrogenase (XDH),[10] which oxidizes xylitol to xylulose using NAD^+. In this system, the substrate xylose, the intermediate xylitol, and the product xylulose would freely diffuse through OmpF, while the essential cofactors NADH and NAD^+ remain encapsulated (Fig. 1).

In earlier work, we assembled a defined number of cascade enzymes on DNA scaffolds by fusing *Pichia stipitis* XR[11] to the modular adaptor ZF-SNAP (ZS),[12] which consists of a monomeric zinc finger protein (zif268)[13] linked to a SNAP tag protein,[14] enabling XR-XDH cascade reaction on 2D or 3D DNA scaffolds.[12] However, ZS-XR exhibited marked loss of activity under the liposome formation condition. To overcome this limitation, we replaced XR with the thermostable TeXR to construct ZS-TeXR (Fig. S1). In parallel, XDH was fused to HG, a modular adaptor composed of a dimeric leucine zipper protein (GCN4)[15] and a HALO tag protein[16] to construct HG-XDH. This strategy enabled stable encapsulation of a defined number of enzymes, allowing us to evaluate cascade performance within a synthetic transporter-equipped compartment.

ZS-TeXR specifically bound to the zif268 recognition sequence and reacted with the SNAP-tag substrate benzylguanine (BG) embedded within the zif268 DNA sequence. Unlike ZS-XR, the activity of ZS-TeXR remained stable for 48 hours (Fig. S2), although its reaction rate was significantly lower than that of ZS-XR in the

[a] *Institute of Advanced Energy, Kyoto University, Uji, Kyoto 611-0011, Japan*
[b] *Department of Health and Nutrition, Kyoto Koka Women's University, Ukyo-ku, Kyoto 615-0882, Japan. E-mail: morii.takashi.68s@st.kyoto-u.ac.jp*

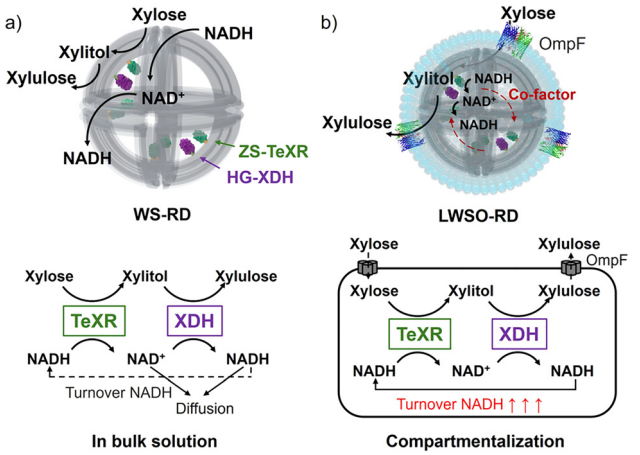

Fig. 1 Schematic illustrations of the enzyme cascade reaction in both a bulk solution and a compartmentalized environment. (a) In a bulk solution, the free diffusion of the intermediate xylitol and the cofactor NAD^+ results in a lower conversion efficiency of the cascade. (b) In a compartmentalized environment, the effective concentrations of enzymes and cofactors are significantly increased. This confinement serves to minimize the diffusion of cofactors into the external solution, thereby enhancing the reaction rate and the efficiency of cofactor recycling in enzymatic reactions.

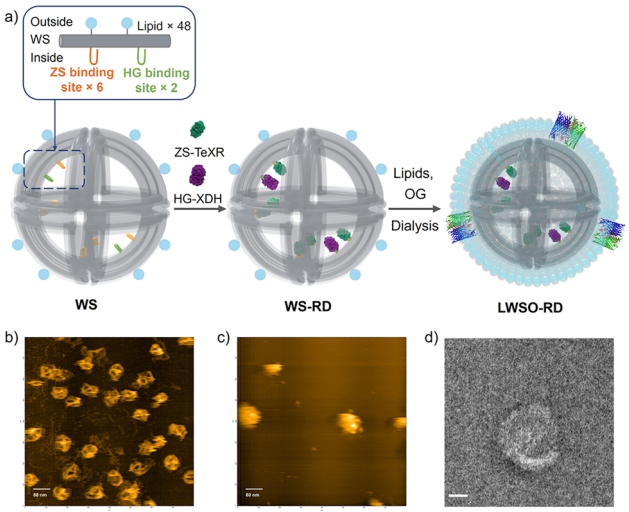

Fig. 2 (a) A scheme illustrating the construction of an artificial compartment containing a defined number of ZS-TeXR and HG-XDH enzymes for a cascade reaction. The DNA origami wireframe skeleton (WS) contains six ZS-binding sites for ZS-TeXR and two HG-binding sites for HG-XDH. After assembling these enzymes onto the WS, lipidated oligonucleotides (ODNs) were attached to the WS in a buffered solution containing surfactant. The resulting hybrid structure was then mixed with surfactant-lipid micelles to form liposomes around the WS (LWS-RD) through a dialysis process that removed the excess surfactant. Finally, OmpF was inserted into the liposome membrane to form the LWSO-RD compartment. (b) AFM images of WS. Scale bar: 80 nm. (c) AFM images of WS-RD. Scale bar: 80 nm. (d) TEM images of LWSO-RD. Scale bar: 20 nm.

presence of 500 μM NADH. Kinetic analysis revealed that ZS-TeXR exhibited a K_m for xylose comparable to ZS-XR[17] (Fig. S3), while the K_m for NADH (3.15 mM) was markedly higher than that of ZS-XR (0.15 mM). Although ZS-TeXR exhibited a higher reaction rate with NADPH than with NADH due to its lower K_m for NADPH than for NADH (Fig. S4), NAD^+ was much preferred to $NADP^+$ as a cofactor for XDH (Fig. S5). Therefore, NADH was used as the initial cofactor in the ZS-TeXR/HG-XDH cascade reaction.

Based on these parameters, the DNA origami skeleton WS was designed with six binding sites for ZS-TeXR and two for HG-XDH (Fig. 2a, b and Fig. S6). DNA strands were modified with BG for ZS-TeXR (Fig. S6) and with chlorohexane (CH) for HG-XDH (Fig. S6). After incubation of WS with ZS-TeXR and/or HG-XDH at a 1 : 2 molar ratio, gel filtration removed unbound proteins and yielded purified WS assembled with both ZS-TeXR and HG-XDH (WS-RD). Enzyme loading was quantified by SDS-PAGE because an AFM imaging was limited by the 3D shape of WS (Fig. 2c and Fig. S7). In the individually assembled system, there are 5 ± 0.2 ZS-TeXR monomers and 1.9 ± 0.3 HG-XDH dimers per WS, WS-R and WS-D, respectively (Fig. S8 and S9). In the co-assembled system, 5.1 ± 0.1 ZS-TeXR monomers and 1.9 ± 0.2 HG-XDH dimers were loaded onto each WS-RD (Fig. S10). No significant difference was observed in the enzyme loading numbers between the individually assembled (WS-R: 5 ± 0.1; WS-D: 2 ± 0.1) and co-assembled systems, indicating that the simultaneous immobilization of ZS-TeXR and HG-XDH did not interfere with their binding efficiency or the structural integrity of the WS scaffold.

In this cascade (Fig. 1), the efficiency can be directly estimated by quantifying xylulose production by XDH. To quantify xylulose, we employed a coupled reaction with xylulose kinase (XK), which converts xylulose to xylulose-5-phosphate by consuming ATP.[17] The amount of ADP yielded from this reaction is the same as the amount of xylulose (Fig. S11a). Verification experiments confirmed that ADP yield correlated closely with NADH production by HG-XDH, with >93% conversion efficiency (Fig. S11). Thus, XK provided a reliable readout of cascade efficiency.

We next evaluated the cascade efficiency of free enzymes and enzymes assembled on WS by monitoring xylulose production (Fig. 1a). Comparison of free and scaffolded enzymes showed modest but reproducible activity enhancement. The initial reaction rate (V_{ini}) of HG-XDH (10 nM) on WS-D (5 nM) was approximately 1.3-fold higher than that of free HG-XDH (10 nM) (Fig. 3a and b). Similarly, ZS-TeXR (25 nM) on WS-R (5 nM) displayed a 1.2-fold increase in V_{ini} over free ZS-TeXR at different NADH concentrations ranging from 500 μM to 4 mM (Fig. 3c and Fig. S13–S15). When both enzymes were co-assembled (WS-RD), cascade activity increased by 1.5-fold relative to free enzymes (Fig. 3d and Fig. S16–S18). These results are consistent with our previous findings that the enzyme catalyzing hydrophilic substrates exhibit higher reaction rates on DNA scaffolds.[18] The cascade reaction efficiency was particularly enhanced at low cofactor levels (Fig. 3d).

To assess the effect of compartmentalization, WS-RD was encapsulated within liposomes containing NADH. The liposome-coated WS-RD (LWS-RD) was purified by density-gradient ultracentrifugation (Fig. S19).[8] The LWS-RD fractions were then incubated with OmpF to form LWSO-RD and analyzed by TEM. TEM images confirmed liposome diameter of 77.8 ± 10.4 nm (n = 172), consistent with the designed diameter of 75 nm (Fig. 2d and Fig. S20).[8] Using our previously established protocol,[8] we quantified the encapsulation yields for LWS, LWS-RD, and LWSO-RD as 83 ± 4%, 79 ± 5%, and 78 ± 4%, respectively (Fig. S21), The high and

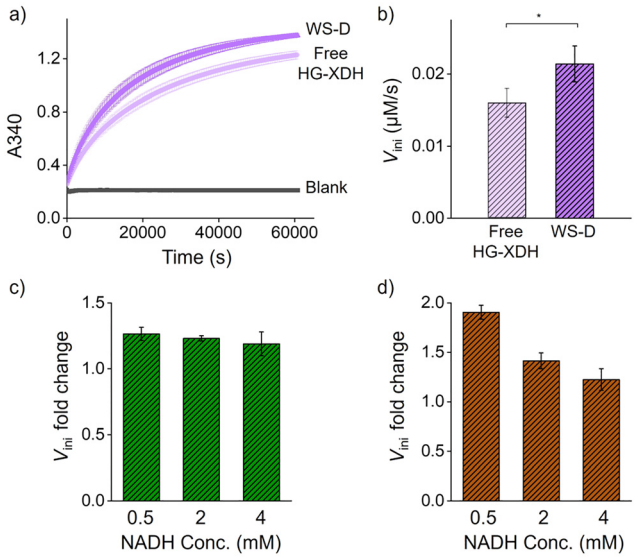

Fig. 3 (a) The time course of the reaction of free HG-XDH (10 nM) and WS-D (5 nM, 10 nM HG-XDH) is monitored by A340. (b) The initial reaction rate of free HG-XDH (10 nM) and WS-D (5 nM, 10 nM HG-XDH) was calculated from the data collected between 0 and 2000 seconds. (c) Fold change in the initial reaction rate (V_{ini}) of ZS-TeXR (25 nM) on WS-R (5 nM) over free ZS-TeXR (25 nM) at different NADH concentrations ranging from 0.5 mM to 4 mM. (d) Fold change in the initial reaction rate (V_{ini}) of cascade enzymes co-assembled on WS (WS-RD) over free enzymes at different NADH concentrations ranging from 0.5 mM to 4 mM.

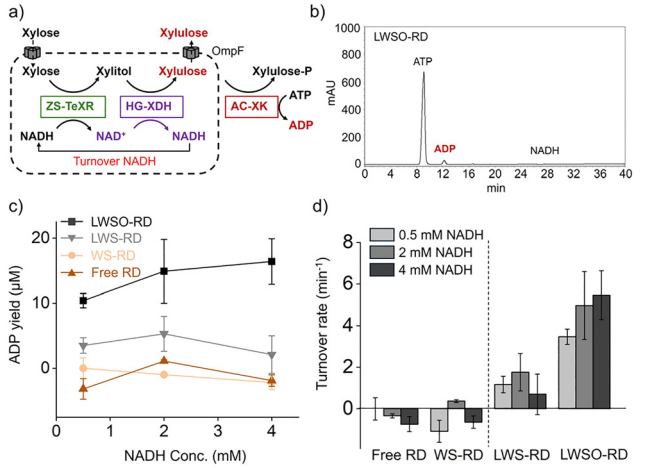

Fig. 4 (a) A schematic diagram illustrates the cascade reaction involving ZS-TeXR and HG-XDH. NADH turnover is evaluated from ADP production in the subsequent AC-XK reaction. (b) An HPLC chromatogram shows the reaction products of LWSO-RD after 10 hours. (c) A comparison of NADH regeneration in the effective NADH concentration for free RD, WS-RD, LWS-RD, and LWSO-RD (see Methods). (d) Turnover numbers for the enzyme cascade reactions for the effective NADH concentration free RD, WS-RD, LWS-RD and LWSO-RD. NADH concentrations are 0.5, 2, and 4 mM in the compartments (LWS-RD and LWSO-RD), and 0.35, 1.4, and 2.7 μM for free RD and WS-RD.

similar encapsulation efficiencies across all constructs, regardless of the presence or absence of anchored proteins, demonstrate that our method is robust and broadly applicable.

Three types of liposomes (LWS-RD and LWSO-RD) were prepared, each encapsulating different concentrations of NADH (500 μM, 2 mM, and 4 mM). Initial internal NADH concentrations of 500 μM, 2 mM, and 4 mM in LWS-RD (5 nM) or LWSO-RD (5 nM) correspond to effective concentration of 0.35, 1.4, and 2.7 μM NADH, respectively, in 100 μL of the cascade reaction mixture (for the details of effective NADH concentration, see "estimation of the effective NADH concentration in the bulk solution" in Methods). Successful internalization of NADH into the liposomes was confirmed by variations in peak intensity that correlated with the initial NADH concentrations (see Fig. S22 and Table S4).

Cascade reactions of free ZS-TeXR and HG-XDH (free RD), WS-RD, LWS-RD, and LWSO-RD (Fig. 1b) were compared under equivalent enzyme and NADH conditions (Fig. 4a). All reaction systems contained an equivalent number of moles of ZS-TeXR and HG-XDH. The initial NADH concentrations were equivalent to those of the liposome-encapsulated NADH.

Each reaction was analyzed by HPLC to quantify the ADP produced at steady state after 10 hours (Fig. 4b and Fig. S23–S25). Monitoring of NADH absorbance and ADP production revealed that only LWSO-RD supported efficient cascade activity (Fig. 4c). At a low internal concentration of NADH (500 μM), the ADP yield was 10 to 15 μM for LWSO-RD. No significant activity was detected for free RD or WS-RD (Fig. 4d). The lack of activity for LWS-RD indicates that OmpF effectively introduces xylose into the LWSO-RD compartment. These results suggest that the cascade reaction is significantly more efficient under compartmentalization than in a bulk solution when the effective concentration of the cofactor NADH is low. This can be attributed to the microenvironment within the liposomes, where local enzyme and NADH concentrations are significantly higher. This accelerates the cascade reaction compared to the free enzyme system.

However, increasing the internal NADH concentration to 2 or 4 mM did not improve the ADP yield in LWSO-RD further (Fig. 4c and Fig. S26). The same trend was observed in the non-liposomal WS-RD reaction (Fig. 3d). Since the Michaelis–Menten kinetics of the ZS-TeXR reaction with 4 mM NADH showed no inhibition at this concentration (Fig. S3), the plateau observed in the efficiency of the cascade reaction could not be explained by ZS-TeXR inhibition at higher internal NADH concentrations. In LWSO-RD, OmpF permits bidirectional flux of xylose, xylitol, and xylulose, though not as freely as in WS-RD. Therefore, intermediates formed in LWSO-RD are prone to escape unless they are transferred directly from ZS-TeXR to HG-XDH. Consequently, the turnover rate of the second step, catalyzed by HG-XDH, remained relatively unchanged. This resulted in little variation in cascade efficiency across different initial NADH concentrations (Fig. 4d). Our results suggest that tuning the stoichiometry and/or spacing of ZS-TeXR and HG-XDH would further improve the efficiency of the cascade reaction in LWSO-RD.

In summary, defined numbers of xylose cascade enzymes, ZS-TeXR and HG-XDH, were successfully assembled on a DNA origami scaffold and encapsulated within liposomes. Incorporation of the size-selective membrane transporter protein

OmpF enabled internal retention of essential cofactors while allowing free diffusion of substrate and intermediate. The compartmentalized system exhibited markedly enhanced cascade efficiency compared to non-compartmentalized enzymes, particularly at low NADH concentrations. The observed plateau in efficiency at higher NADH levels suggests that enzyme stoichiometry and spacing critically influence the performance of the cascade, even within confined compartments. It should be noted that there are potential limitations to our enzyme anchoring strategy. Although the modular adaptor provides covalent stability and a high assembly yield, it may restrict the conformational flexibility of enzymes tethered to the DNA scaffold in some cases. This could lead to suboptimal orientations and contribute to the activity plateau observed at high enzyme densities. This effect is likely enzyme-dependent, as the catalytic performance of ZS-TeXR was more constrained than that of HG-XDH, possibly due to the structural sensitivity of TeXR itself. The current arrangement of enzymes is not a fixed limitation, but rather a deliberate design choice. Both stoichiometry and inter-enzyme spacing can be easily modified by changing the number and locations of binding sites through staple strand redesign. This inherent programmability highlights the adaptability of our platform for systematically investigating how spatial organization influences cascade reactions. Future studies manipulating inter-enzyme spacing and stoichiometry in our compartmentalized systems will further illuminate the design principles of efficient enzymatic cascades. These studies will also advance applications in synthetic biology and biocatalysis.

This work was supported by JSPS KAKENHI, Grant Numbers 23H02083 and 23K26776 (T. M.), 24K17787 (P. L.), 24H01129 and 24K01629 (E. N.), Japan. The TEM measurements in this study were supported by the Kyoto University Nano Technology Hub in the "Nanotechnology Platform Project," sponsored by MEXT, Japan. The Analysis and Development System for Advanced Materials (ADAM) at the Research Institute for Sustainable Humanosphere (RISH) of Kyoto University also supported this study.

Conflicts of interest

There are no conflicts to declare.

Data availability

The data supporting this article have been included as part of the supplementary information (SI). Supplementary information is available. See DOI: https://doi.org/10.1039/d5cc06049d.

Notes and references

1 (*a*) A. H. Chen and P. A. Silver, *Trends Cell Biol.*, 2012, **22**, 662–670; (*b*) H. Eichelmann, E. Talts, V. Oja, E. Padu and A. Laisk, *J. Exp. Bot*, 2009, **60**, 4077–4088; (*c*) K. Jørgensen, A. V. Rasmussen, M. Morant, A. H. Nielsen, N. Bjarnholt, M. Zagrobelny, S. Bak and B. L. Møller, *Curr. Opin. Plant Biol.*, 2005, **8**, 280–291; (*d*) B. A. Manjasetty, J. Powlowski and A. Vrielink, *Proc. Natl. Acad. Sci. U. S. A.*, 2003, **100**, 6992–6997; (*e*) Y. Liu, L. L. Beer and W. B. Whitman, *Trends Microbiol.*, 2012, **20**, 251–258.

2 (*a*) S. Hurtley, *Science*, 2009, **326**, 1205; (*b*) C. A. Kerfeld, M. R. Sawaya, S. Tanaka, C. V. Nguyen, M. Phillips, M. Beeby and T. O. Yeates, *Science*, 2005, **309**, 936–938; (*c*) I. A. Berlatzky, A. Rouvinski and S. Ben-Yehuda, *Proc. Natl. Acad. Sci. U. S. A.*, 2008, **105**, 14136–14140; (*d*) A. Küchler, M. Yoshimoto, S. Luginbühl, F. Mavelli and P. Walde, *Nat. Nanotechnol.*, 2016, **11**, 409–420.

3 B. H. Lipshutz, N. A. Isley, J. C. Fennewald and E. D. Slack, *Angew. Chem., Int. Ed.*, 2013, **52**, 10952–10958.

4 (*a*) Y. A. Takagi, D. H. Nguyen, T. B. Wexler and A. D. Goldman, *J. Mol. Evol.*, 2020, **88**, 598–617; (*b*) S. Koga, D. S. Williams, A. W. Perriman and S. Mann, *Nat. Chem.*, 2011, **3**, 720–724; (*c*) J. P. Schrum, T. F. Zhu and J. W. Szostak, *Cold Spring Harb. Perspect. Biol.*, 2010, **2**, a002212.

5 (*a*) O. Staufer, M. Schröter, I. Platzman and J. P. Spatz, *Small*, 2020, **16**, 1906424; (*b*) C. D. Reinkemeier, G. E. Girona and E. A. Lemke, *Science*, 2019, **363**, eaaw2644; (*c*) E. Rideau, R. Dimova, P. Schwille, F. R. Wurm and K. Landfester, *Chem. Soc. Rev.*, 2018, **47**, 8572–8610; (*d*) B. C. Buddingh and J. C. M. Van Hest, *Acc. Chem. Res.*, 2017, **50**, 769–777; (*e*) S. Kumar, M. Karmacharya, I. J. Michael, Y. Choi, J. Kim, I. Kim and Y. K. Cho, *Nat. Catal.*, 2021, **4**, 763–774.

6 J. Fu, M. Liu, Y. Liu, N. W. Woodbury and H. Yan, *J. Am. Chem. Soc.*, 2012, **134**, 2023.

7 (*a*) Z. G. Wang, O. I. Wilner and I. Willner, *Nano Lett.*, 2009, **9**, 4098–4102; (*b*) L. Sun, Y. Gao, Y. Xu, J. Chao, H. Liu, L. Wang, D. Li and C. Fan, *J. Am. Chem. Soc.*, 2017, **139**, 17525–17532; (*c*) G. Ke, M. Liu, S. Jiang, X. Qi, Y. R. Yang, S. Wooten, F. Zhang, Z. Zhu, Y. Liu, C. J. Yang and H. Yan, *Angew. Chem.*, 2016, **128**, 7609–7612; (*d*) V. Linko, M. Eerikäinen and M. A. Kostiainen, *Chem. Commun.*, 2015, **51**, 5351–5354.

8 (*a*) S. Zhang, E. Nakata, P. Lin and T. Morii, *Chem. – Eur. J.*, 2023, **29**, e202302093; (*b*) S. Zhang, P. Lin, F. Komatsubara, E. Nakata and T. Morii, *ChemBioChem*, 2025, **26**, e202401041.

9 S. Fernandes, M. G. Tuohy and P. G. Murray, *J. Biosci.*, 2009, **34**, 881–890.

10 S. Watanabe, T. Kodaki and K. Makino, *J. Biol. Chem.*, 2005, **280**, 10340–10349.

11 S. Watanabe, A. Abu Saleh, S. P. Pack, N. Annaluru, T. Kodaki and K. Makino, *Microbiology*, 2007, **153**, 3044–3054.

12 (*a*) T. A. Ngo, E. Nakata, M. Saimura and T. Morii, *J. Am. Chem. Soc.*, 2016, **138**, 3012–3021; (*b*) P. Lin, H. Dinh, Y. Morita, E. Nakata and T. Morii, *Adv. Funct. Mater.*, 2023, **33**, 2215023.

13 (*a*) N. P. Pavletich and C. O. Pabo, *Science*, 1991, **252**, 809; (*b*) E. Nakata, F. F. Liew, C. Uwatoko, S. Kiyonaka, Y. Mori, Y. Katsuda, M. Endo, H. Sugiyama and T. Morii, *Angew. Chem., Int. Ed.*, 2012, **51**, 2421–2424.

14 (*a*) A. Keppler, S. Gendreizig, T. Gronemeyer, H. Pick, H. Vogel and K. Johnsson, *Nat. Biotechnol.*, 2003, **21**, 86; (*b*) E. Nakata, H. Dinh, T. A. Ngo, M. Saimura and T. Morii, *Chem. Commun.*, 2014, **51**, 1016–1019; (*c*) T. M. Nguyen, E. Nakata, M. Saimura, H. Dinh and T. Morii, *J. Am. Chem. Soc.*, 2017, **139**, 8487–8496; (*d*) T. M. Nguyen, E. Nakata, Z. Zhang, M. Saimura, H. Dinh and T. Morii, *Chem. Sci.*, 2019, **10**, 9315–9325; (*e*) Z. Zhang, E. Nakata, H. Dinh, M. Saimura, A. Rajendran, K. Matsuda and T. Morii, *Chem. – Eur. J.*, 2021, **27**, 18118–18128.

15 T. E. Ellenberger, C. J. Brandl, K. Struhl and S. C. Harrison, *Cell*, 1992, **71**, 1223–1237.

16 C. G. England, H. Luo and W. Cai, *Bioconjugate Chem.*, 2015, **26**, 975–986.

17 P. Lin, H. Dinh, E. Nakata and T. Morii, *Chem. Commun.*, 2021, **57**, 11197–11200.

18 P. Lin, T. Hayashi, H. Dinh, E. Nakata, M. Kinoshita and T. Morii, *ACS Appl. Mater. Interfaces*, 2025, **17**, 15775–15792.

